

## Noise and vibration emerging methods

The 6th conference, 7 – 9 May 2018 Ibiza – Spain

# ENERGY EXCHANGE BETWEEN TWO SUB-SYSTEMS COUPLED WITH A NONLINEAR ELASTIC PATH

Osman Taha Sen<sup>1\*</sup> and Rajendra Singh<sup>2</sup>

<sup>1</sup>Mechanical Engineering Department, Istanbul Technical University, Istanbul, TURKEY \*Email: <a href="mailto:senos@itu.edu.tr">senos@itu.edu.tr</a>

<sup>2</sup>Department of Mechanical and Aerospace Engineering, The Ohio State University, Columbus, Ohio, USA

#### **ABSTRACT**

The chief objective of this paper is to explore energy transfer mechanism between the subsystems that are coupled by a nonlinear elastic path. In the proposed model (via a minimal order, two degree of freedom system), both sub-systems are defined as damped harmonic oscillators with linear springs and dampers. The first sub-system is attached to the ground on one side but connected to the second sub-system on the other side. In addition, linear elastic and dissipative characteristics of both oscillators are assumed to be identical, and a harmonic force excitation is applied only on the mass element of second oscillator. The nonlinear spring (placed in between the two sub-systems) is assumed to exhibit cubic, hardening type nonlinearity. First, the governing equations of the two degree of freedom system with a nonlinear elastic path are obtained. Second, the nonlinear differential equations are solved with a semi-analytical (multi-term harmonic balance) method, and nonlinear frequency responses of the system are calculated for different path coupling cases. As such, the nonlinear path stiffness is gradually increased so that the stiffness ratio of nonlinear element to the linear element is 0.01, 0.05, 0.1, 0.5 and 1.0 while the absolute value of linear spring stiffness is kept intact. In all solutions, it is observed that the frequency response curves at the vicinity of resonant frequencies bend towards higher frequencies as expected due to the hardening effect. However, at moderate or higher levels of path coupling (say 0.1, 0.5 and 1.0), additional branches emerge in the frequency response curves but only at the first resonant frequency. This is due to higher displacement amplitudes at the first resonant frequency as compared to the second one. Even though the oscillators move in-phase around the first natural frequency, high amplitudes increase the contribution of the stored potential energy in the nonlinear spring to the total mechanical energy. The out-of-phase motion around the second natural frequency

cannot significantly contribute due to very low motion amplitudes. Finally, the governing equations are numerically solved for the same levels of nonlinearity, and the motion responses of both sub-systems are calculated. Both in-phase and out-of-phase motion responses are successfully shown in numerical solutions, and phase portraits of the system are generated in order to illustrate its nonlinear dynamics. In conclusion, a better understanding of the effect of nonlinear elastic path on two damped harmonic oscillators is gained.

#### 1 INTRODUCTION

The focus of this paper is on two linear sub-systems that are coupled via a nonlinear path. Accordingly, the objectives are: 1) Develop a model of the coupled system and obtain corresponding nonlinear governing equations; 2) Solve the governing equations in frequency domain with a semi-analytical approach, and generate nonlinear frequency response curves for different levels of nonlinearity; 3) Calculate the time domain solutions of the system to identify periodic responses with different excitation frequencies and nonlinearity levels, and investigate the dynamic behavior of both sub-systems.

Prior work on this topic includes a study by Starosvetsky and Gendelman [1] who examined the energy absorbing mechanism of a nonlinear energy sink attached to a two degree of freedom linear system. It was observed that the nonlinear absorber is favorable at higher amplitude excitations and inefficient at lower amplitude excitations. Furthermore, additional branches in frequency response curves were detected at lower amplitude excitation cases. In another study, Kurt et al. [2] investigated two weakly damped oscillators that are coupled through a weak elastic element. The results were displayed in terms of frequency-energy plots, and various branches were identified. Jiang et al. [3] examined a similar system using analytical and experimental methods. They showed that the energy of the primary system can be effectively absorbed by the secondary system when the coupling between them is nonlinear. Thus, the vibration amplitudes of the primary system could be minimized over a broad frequency range. Andersen et al. [4] developed a two degree of freedom system where all elastic and dissipative elements are linear but this system exhibited geometric nonlinearity due to the angular configurations of springs and dampers; the system may be dynamically unstable due to its kinematics.

## 2 PROBLEM FORMULATION

For the sake of simplicity, two damped harmonic oscillators are coupled via a nonlinear elastic spring  $(k_{nl})$  as shown in Figure 1. For the two degree of freedom system, it is assumed that both oscillators are identical, possessing the same inertial (m), dissipative (c) and elastic (k) characteristics though the first oscillator is grounded on one end while the mass of the second oscillator is free on the other end. An external dynamic force,  $F(t) = A \sin(\omega t + \phi)$ , is applied on the second mass as illustrated in Figure 1.

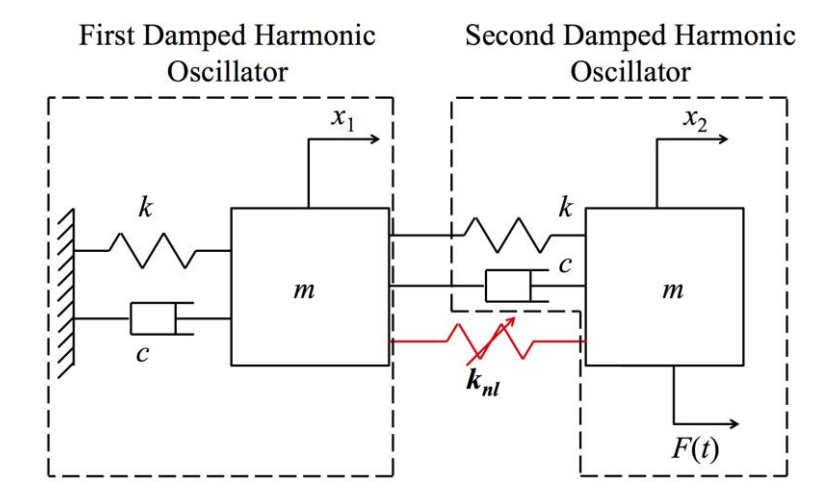


Figure 1: Two degree of freedom damped system illustrating two sub-systems that are coupled via a nonlinear spring  $(k_{nl})$ .

The nonlinear elastic path is assumed to exhibit cubic nonlinearity. Thus, the nonlinear governing equations of the system of Figure 1 are:

$$m\ddot{x}_1 + 2c\dot{x}_1 - c\dot{x}_2 + 2kx_1 - kx_2 - k_{nl}(x_2 - x_1)^3 = 0,$$

$$m\ddot{x}_2 + c\dot{x}_2 - c\dot{x}_1 + kx_2 - kx_1 + k_{nl}(x_2 - x_1)^3 = F(t).$$
(1)

$$m\ddot{x}_2 + c\dot{x}_2 - c\dot{x}_1 + kx_2 - kx_1 + k_{nl}(x_2 - x_1)^3 = F(t). \tag{2}$$

In order to simplify the above governing equations, the following non-dimensional parameters are defined:

$$\omega_n = \sqrt{k/m}, \quad \zeta = c/2m\omega_n, \quad \tau = \omega_n t, \quad x_0 = A/k,$$
 $X_1 = x_1/x_0, \quad X_2 = x_2/x_0, \quad \alpha = k_{nl}x_0^2/k.$  (3a-g)

Hence, the nonlinear governing equations are obtained in non-dimensional form as follows:

$$X_1'' + 4\zeta X_1' - 2\zeta X_2' + 2X_1 - X_2 - \alpha (X_2 - X_1)^3 = 0, \tag{4}$$

$$X_2'' + 2\zeta X_2' - 2\zeta X_1' + X_2 - X_1 + \alpha (X_2 - X_1)^3 = \sin\left(\frac{\omega}{\omega_n}\tau + \phi\right),\tag{5}$$

where  $X_i' = dX_i/d\tau$  and  $X_i'' = d^2X_i/d\tau^2$ .

## NONLINEAR FREQUENCY RESPONSES USING SEMI-ANALYTICAL **METHOD**

The multi-term harmonic balance method (MHBM) is applied to construct the steady-state response of the nonlinear system excited by a harmonic function. In order to simplify the formulation, first the nonlinear governing equations (Eqs. (4-5)) are transformed to spatial domain with a linear independent variable transformation,  $\theta = \omega \tau$ . Consequently, the derivatives with respect to  $\tau$  in Eqs. (4) and (5) are defined again with respect to the new independent variable  $\theta$ . As a result, the following nonlinear governing equations are obtained in  $\theta$  domain:

$$\omega^2 \frac{\mathrm{d}^2 X_1}{\mathrm{d}\theta^2} + 4\zeta \omega \frac{\mathrm{d}X_1}{\mathrm{d}\theta} - 2\zeta \omega \frac{\mathrm{d}X_2}{\mathrm{d}\theta} + 2X_1 - X_2 - \alpha (X_2 - X_1)^3 = 0, \tag{6}$$

$$\omega^{2} \frac{d^{2} X_{2}}{d\theta^{2}} + 2\zeta \omega \frac{dX_{2}}{d\theta} - 2\zeta \omega \frac{dX_{1}}{d\theta} + X_{2} - X_{1} + \alpha (X_{2} - X_{1})^{3} = \sin \left(\frac{1}{\omega_{n}}\theta + \phi\right). \tag{7}$$

The solutions for the non-dimensional dependent variables  $X_1$  and  $X_2$  are assumed in the forms of truncated Fourier series where  $N_h$  represents the number of harmonics retained in the expansion:

$$X_{1}(\theta) = a_{1,0} + \sum_{n=1}^{N_{h}} a_{1,2n-1} \sin(n\theta) + a_{1,2n} \cos(n\theta),$$
 (8a)  

$$X_{2}(\theta) = a_{2,0} + \sum_{n=1}^{N_{h}} a_{2,2n-1} \sin(n\theta) + a_{2,2n} \cos(n\theta).$$
 (8b)

$$X_2(\theta) = a_{2,0} + \sum_{n=1}^{N_h} a_{2,2n-1} \sin(n\theta) + a_{2,2n} \cos(n\theta).$$
 (8b)

The assumed solutions given with Eqs. (8a) and (8b) are discretized as  $X_1 = \Gamma a_1$  and  $X_2 = \Gamma a_2$ where  $\Gamma$  is the discrete Fourier transform matrix, and  $a_1$  and  $a_2$  are the unknown Fourier coefficient vectors of the dependent variables  $x_1$  and  $x_2$ , respectively. For the discretization process, the matrix  $\Gamma$  is defined as:

$$\Gamma = \begin{bmatrix}
1 & \sin(\theta_0) & \cos(\theta_0) & \cdots & \sin(N_h \theta_0) & \cos(N_h \theta_0) \\
1 & \sin(\theta_1) & \cos(\theta_1) & \cdots & \sin(N_h \theta_1) & \cos(N_h \theta_1) \\
\vdots & \vdots & \vdots & \ddots & \vdots & \vdots \\
1 & \sin(\theta_{N-1}) & \cos(\theta_{N-1}) & \cdots & \sin(N_h \theta_{N-1}) & \cos(N_h \theta_{N-1})
\end{bmatrix},$$
(9)

where N is the number of discrete points. Here, it should be noted that the condition  $N \ge 2N_h$ should be satisfied in order to prevent any aliasing problems. Furthermore, the non-dimensional governing equations (Eqs. (6-7)) are written in discrete form as:

$$\omega^{2}\Gamma \mathbf{D}^{2}\mathbf{a}_{1} + 4\zeta\omega\Gamma \mathbf{D}\mathbf{a}_{1} - 2\zeta\omega\Gamma \mathbf{D}\mathbf{a}_{2} + 2\Gamma\mathbf{a}_{1} - \Gamma\mathbf{a}_{2} - \alpha(\Gamma\mathbf{a}_{2} - \Gamma\mathbf{a}_{1})^{3} = 0,$$

$$\omega^{2}\Gamma \mathbf{D}^{2}\mathbf{a}_{2} + 2\zeta\omega\Gamma \mathbf{D}\mathbf{a}_{2} - 2\zeta\omega\Gamma \mathbf{D}\mathbf{a}_{1} + \Gamma\mathbf{a}_{2} - \Gamma\mathbf{a}_{1} + \alpha(\Gamma\mathbf{a}_{2} - \Gamma\mathbf{a}_{1})^{3} = \Gamma\mathbf{Q},$$
(10)

where  $\bf D$  is the differential operator and  $\bf Q$  is the Fourier coefficients vector for the external force excitation. The differential operator matrix is defined as:

$$\mathbf{D} = \begin{bmatrix} 0 & 0 & 0 & \cdots & 0 & 0 \\ 0 & 0 & -1 & \cdots & 0 & 0 \\ 0 & 1 & 0 & \cdots & 0 & 0 \\ \vdots & \vdots & \vdots & \ddots & \vdots & \vdots \\ 0 & 0 & 0 & \cdots & 0 & -N_h \\ 0 & 0 & 0 & \cdots & N_h & 0 \end{bmatrix}. \tag{12}$$

Observe that, Eqs. (10) and (11) are a set of coupled nonlinear algebraic equations. Hence, the unknowns  $\mathbf{a}_1$  and  $\mathbf{a}_2$  are calculated by minimizing the following residue functions:

$$\mathbf{R}_{1} = \omega^{2} \mathbf{D}^{2} \mathbf{a}_{1} + 4\zeta \omega \mathbf{D} \mathbf{a}_{1} - 2\zeta \omega \mathbf{D} \mathbf{a}_{2} + 2\mathbf{a}_{1} - \mathbf{a}_{2} - \alpha \mathbf{\Gamma}^{+} (\mathbf{\Gamma} \mathbf{a}_{2} - \mathbf{\Gamma} \mathbf{a}_{1})^{3},$$
(13)  
$$\mathbf{R}_{2} = \omega^{2} \mathbf{D}^{2} \mathbf{a}_{2} + 2\zeta \omega \mathbf{D} \mathbf{a}_{2} - 2\zeta \omega \mathbf{D} \mathbf{a}_{1} + \mathbf{a}_{2} - \mathbf{a}_{1} + \alpha \mathbf{\Gamma}^{+} (\mathbf{\Gamma} \mathbf{a}_{2} - \mathbf{\Gamma} \mathbf{a}_{1})^{3} - \mathbf{Q},$$
(14)

where  $\Gamma^+$  is the pseudo-inverse of the discrete Fourier transform matrix,  $\Gamma^+ = (\Gamma^T \Gamma)^{-1} \Gamma^T$ . The residue minimization is done with Newton-Raphson scheme iteratively where  $\mathbf{\eta} = [\mathbf{a}_1 \ \mathbf{a}_2 \ \omega]^T$  and  $\mathbf{R} = [\mathbf{R}_1 \ \mathbf{R}_2]^T$  are the vectors of unknowns and residue, respectively, and *i* is the iteration index:

$$\mathbf{\eta}_{i+1} = \mathbf{\eta}_i - \mathbf{J}_i^{-1} \mathbf{R}_i. \tag{15}$$

Observe that the excitation frequency  $\omega$  is also treated as an unknown in the Newton-Raphson scheme. Hence, the dynamic behavior of the system at the turning points of the frequency response curve is better understood. Furthermore, the matrix **J** in Eq. (15) is the Jacobian matrix and defined as follows:

$$J = \begin{bmatrix} \frac{\partial \mathbf{R}_1}{\partial \mathbf{a}_1} & \frac{\partial \mathbf{R}_1}{\partial \mathbf{a}_2} & \frac{\partial \mathbf{R}_1}{\partial \omega} \\ \frac{\partial \mathbf{R}_2}{\partial \mathbf{a}_1} & \frac{\partial \mathbf{R}_2}{\partial \mathbf{a}_2} & \frac{\partial \mathbf{R}_2}{\partial \omega} \end{bmatrix}$$
(16)

Based on the residue minimization procedure of Eq. (15), Eqs. (13) and (14) are solved iteratively for selected values of parameter  $\alpha$  and the calculated nonlinear frequency response curves are displayed in Figures 2 and 3. The response of the first sub-system ( $X_1$ ) is shown in Figures 2(a) and 2(b) in the vicinity of first and second natural frequencies, respectively. Note that the natural frequencies mentioned are defined in terms the linear system when  $\alpha = 0$ . As seen in Figure 2(a), the backbone response curve simply bends towards higher frequencies at lower  $\alpha$  values ( $\alpha = 0.0001$  and  $\alpha = 0.0005$ ). This result is expected for a weak hardening type nonlinearity. However, as the value of  $\alpha$  is increased, the effect of nonlinearity on the system dynamics becomes more pronounced, thereby generating additional branches. But, the emergence of additional branches is not observed at the vicinity of the second natural frequency (Figure 2(b)). Over this frequency range, only a simple bending of the backbone curve towards higher frequencies is seen. Obviously, the backbone curve bends more as the value of  $\alpha$  is increased. Similar claims can be made regarding the response of the second sub-system as illustrated in Figures 3(a) and 3(b). Again, additional branches emerge only in the vicinity of the first natural frequency and the effect of nonlinearity is pronounced with an increase in  $\alpha$ .

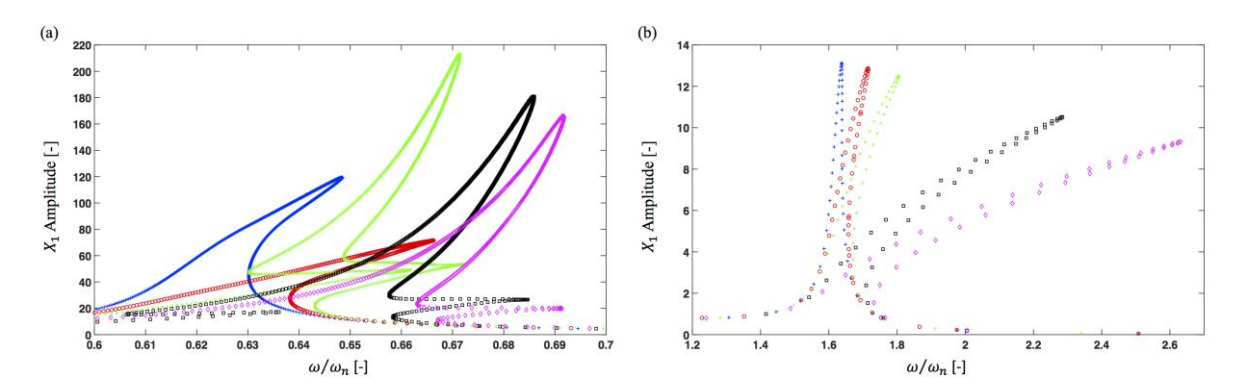


Figure 2: Nonlinear frequency response curves of the first sub-system. (a) Around the first natural frequency; (b) Around the second natural frequency. Key: +,  $\alpha = 0.0001$ ,  $\bigcirc$ ,  $\alpha = 0.0005$ ,  $\times$ ,  $\alpha = 0.001$ ,  $\square$ ,  $\alpha = 0.005$ ,  $\Diamond$ ,  $\alpha = 0.01$ .

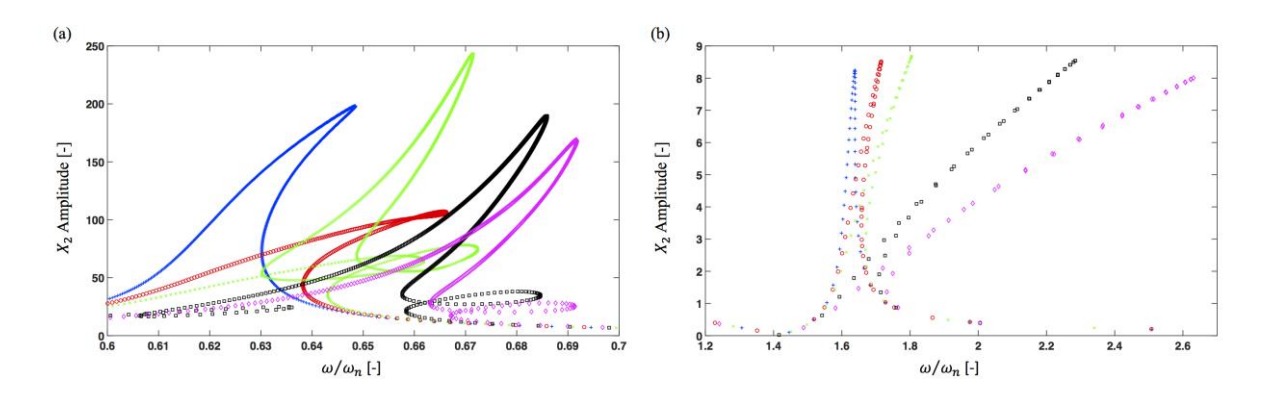


Figure 3: Nonlinear frequency response curves of the second sub-system. (a) Around the first natural frequency; (b) Around the second natural frequency. Key: +,  $\alpha = 0.0001$ ,  $\bigcirc$ ,  $\alpha = 0.0005$ ,  $\times$ ,  $\alpha = 0.001$ ,  $\square$ ,  $\alpha = 0.005$ ,  $\Diamond$ ,  $\alpha = 0.01$ .

## 4 PHASE PORTRAITS BASED ON NUMERICAL SOLUTIONS

To further understand the dynamic behavior, the non-dimensional governing equations (Eqs. (4) and (5)) are numerically solved at selected values of  $\omega$  and  $\alpha$ . As an example, system with the strongest nonlinearity ( $\alpha=0.01$ ) is first investigated at three different values of non-dimensional frequency. The first study is carried around  $\omega/\omega_n=0.677$  which corresponds to a point on the stable branch in the nonlinear frequency response curve. The second non-dimensional frequency is chosen as  $\omega/\omega_n=0.692$ , which is indeed the turning point where the solutions move from a stable branch to an unstable branch. Finally, the last non-dimensional frequency is  $\omega/\omega_n=0.663$ , which corresponded to another turning point where the solutions move from an unstable branch to a stable branch. Corresponding phase portrait of the relative motion between two sub-systems  $(X_1-X_2 \text{ vs. } \dot{X}_1-\dot{X}_2)$  and kinetic energies are displayed in Figures 4, 5 and 6.

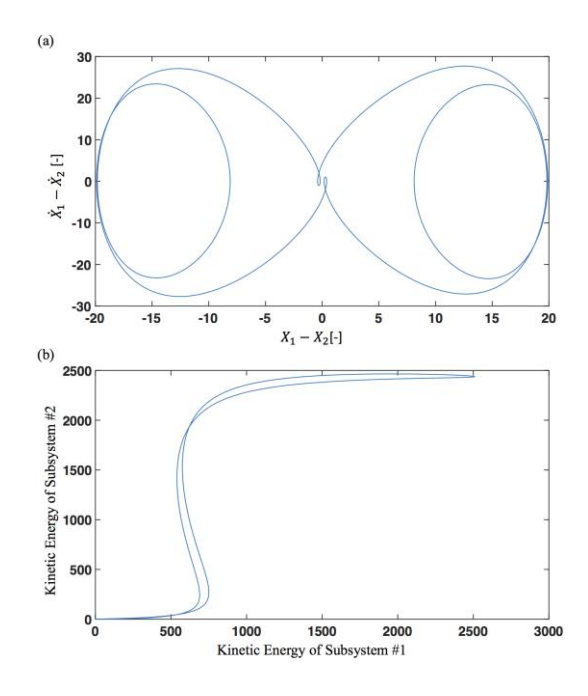


Figure 4: Phase portraits of the system for  $\alpha = 0.01$  at  $\omega/\omega_n = 0.677$ . (a) Phase portrait of relative motion between 2 sub-systems; (b) Phase portrait of kinetic energies.

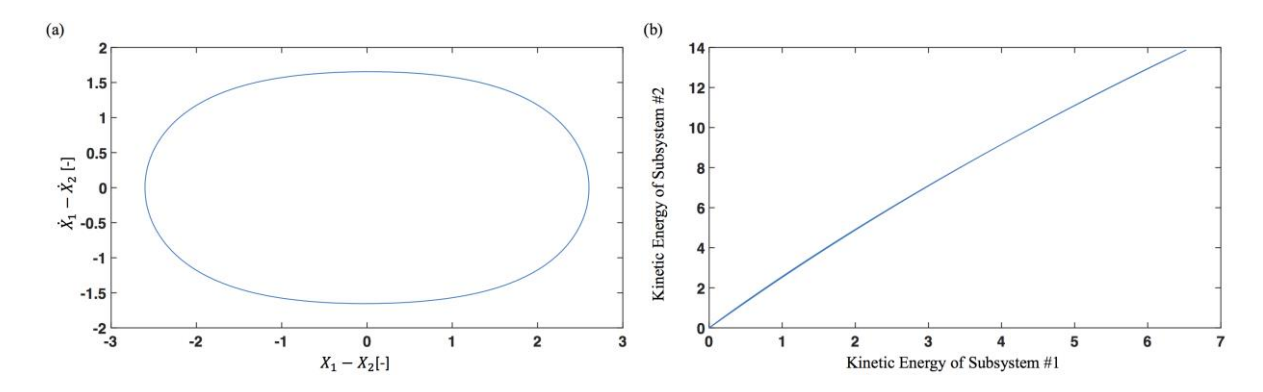


Figure 5: Phase portraits of the system for  $\alpha = 0.01$  at  $\omega/\omega_n = 0.692$ . (a) Phase portrait of relative motion between 2 sub-systems; (b) Phase portrait of kinetic energies.

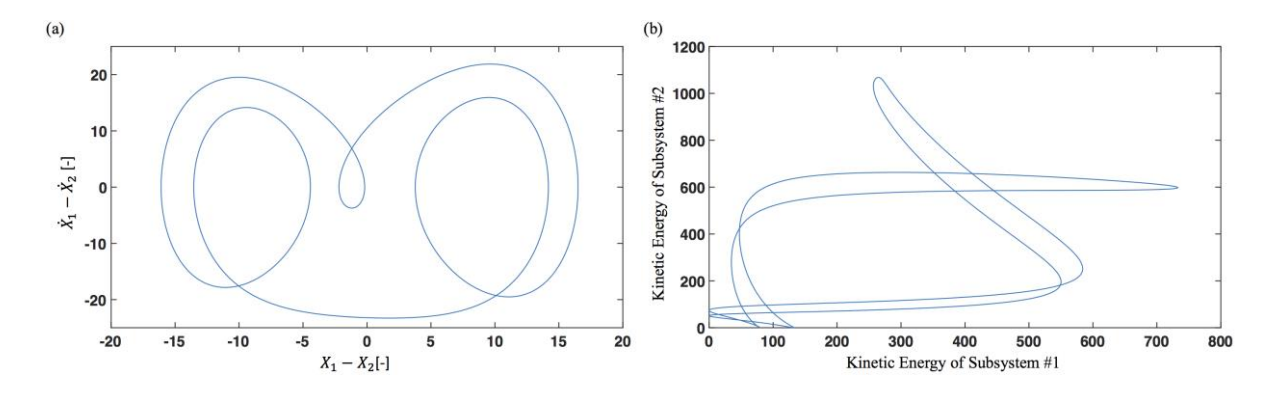


Figure 6: Phase portraits of the system for  $\alpha = 0.01$  at  $\omega/\omega_n = 0.663$ . (a) Phase portrait of relative motion between 2 sub-systems; (b) Phase portrait of kinetic energies.

The system exhibits limit cycle behavior for all frequencies as seen from Figures 4-6. Furthermore, period doubling (or halving) also occurs as the excitation frequency is changed. From the kinetic energy perspective, several observations can be made. The system exhibits different regimes within one period as seen in Figure 4(b). At the lower and higher energy levels, the kinetic energy of the first sub-system changes, but it is almost constant for the second sub-system. Further, at a certain kinetic energy level of the first sub-system, the kinetic energy of the second sub-system changes, while the first sub-system stays at almost constant energy level. The behavior at the vicinity of the first turning point is simpler (Figure 5(b)), i.e. kinetic energies of both systems change concurrently. More complex behavior is indeed seen for the last case (Figure 6(b)). Observe that at some part of the period, kinetic energy of one sub-system increases while the kinetic energy of the other sub-system decreases, and at some part of the period the kinetic energy of the first system changes while the kinetic energy of the second subsystem stays intact.

The phase portraits are depicted in Figures 7, 8, 9 and 10 for weakly ( $\alpha = 0.0001$ ) and strongly ( $\alpha = 0.01$ ) nonlinear cases. Observe that solutions are obtained at several values of  $\omega$ , and corresponding phase portraits of relative motion are given in Figures 7(a)-10(a). Likewise, the phase portraits of the kinetic energies are shown in Figures 7(b)-10(b). First, the system response is always similar around the second natural frequency irrespective of the level of nonlinearity (Figures 8 and 10). Second, the kinetic energy change in sub-systems occurs consecutively at a weaker nonlinearity. In other words, while the kinetic energy of one sub-system changes, the kinetic energy of the other one is intact (Figure 7). However, the kinetic energy exchange mechanism becomes more complex at stronger nonlinearities (Figure 9) as explained previously.

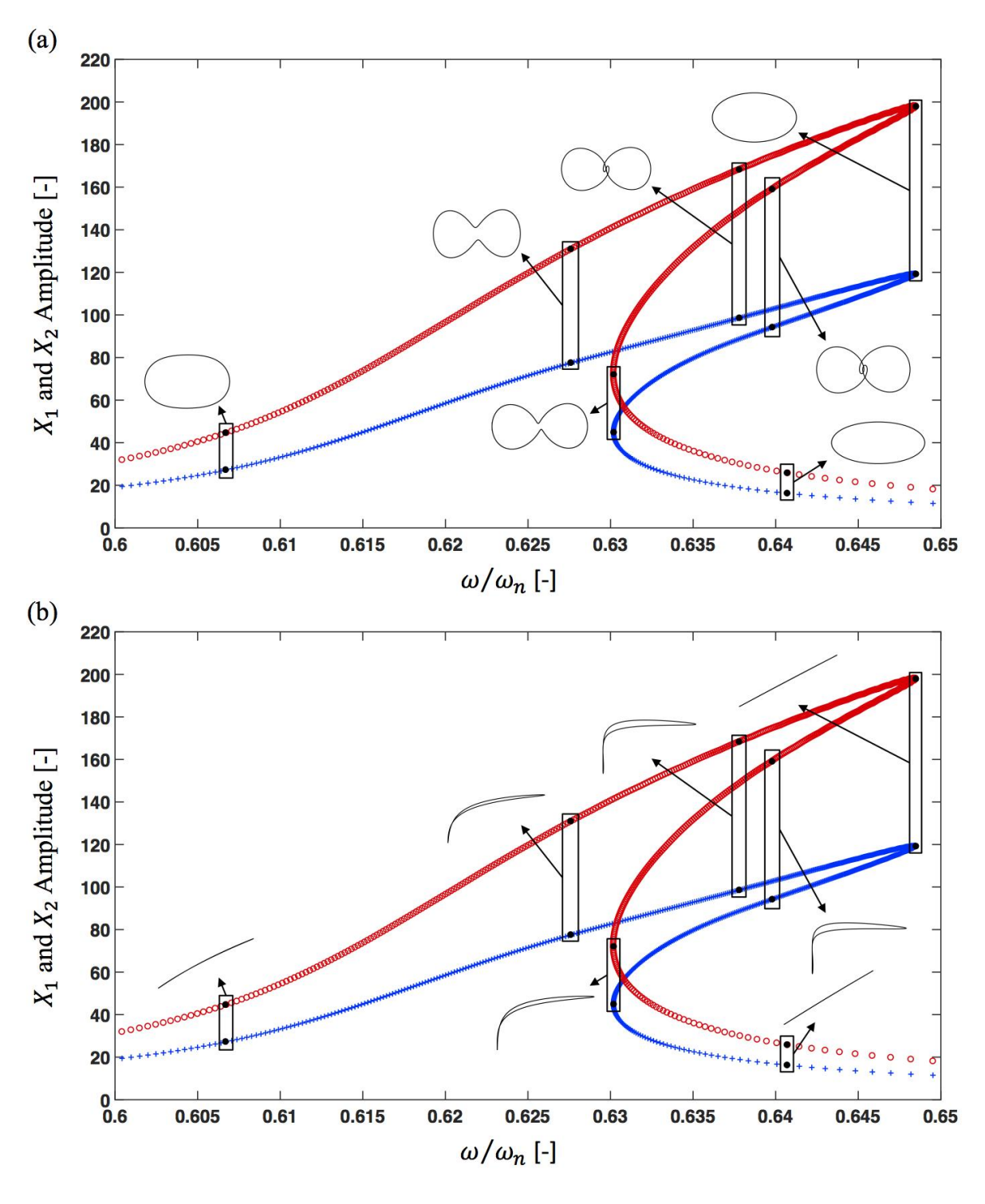


Figure 7: Nonlinear frequency response curves in the vicinity of first natural frequency for  $\alpha = 0.0001$ . (a) Phase portraits of relative motion; (b) Phase portraits of kinetic energies. Key: +,  $X_1$  amplitude, O,  $X_2$  amplitude.

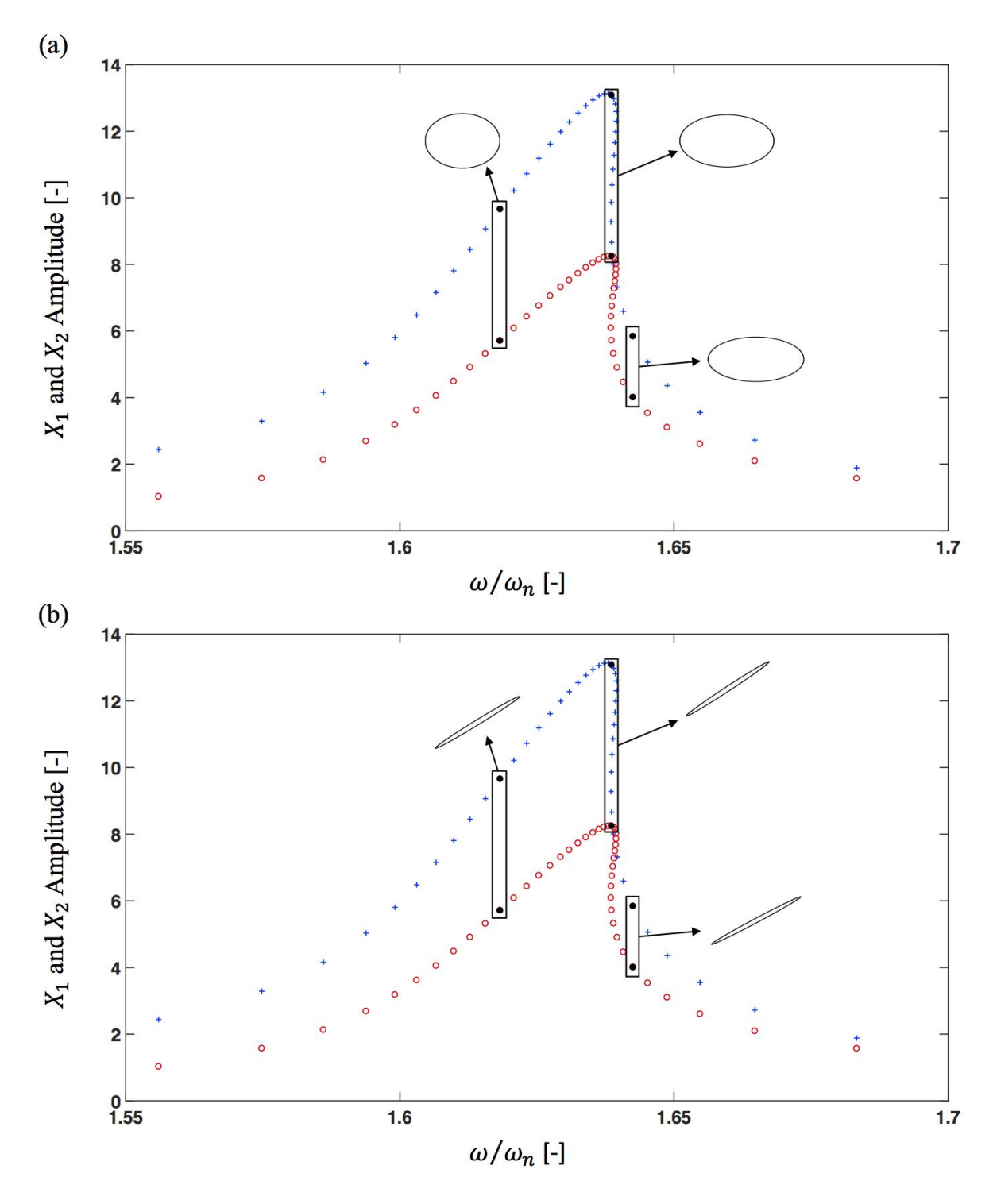


Figure 8: Nonlinear frequency response curves in the vicinity of second natural frequency for  $\alpha = 0.0001$ . (a) Phase portraits of relative motion; (b) Phase portraits of kinetic energies. Key: +,  $X_1$  amplitude,  $\bigcirc$ ,  $X_2$  amplitude.

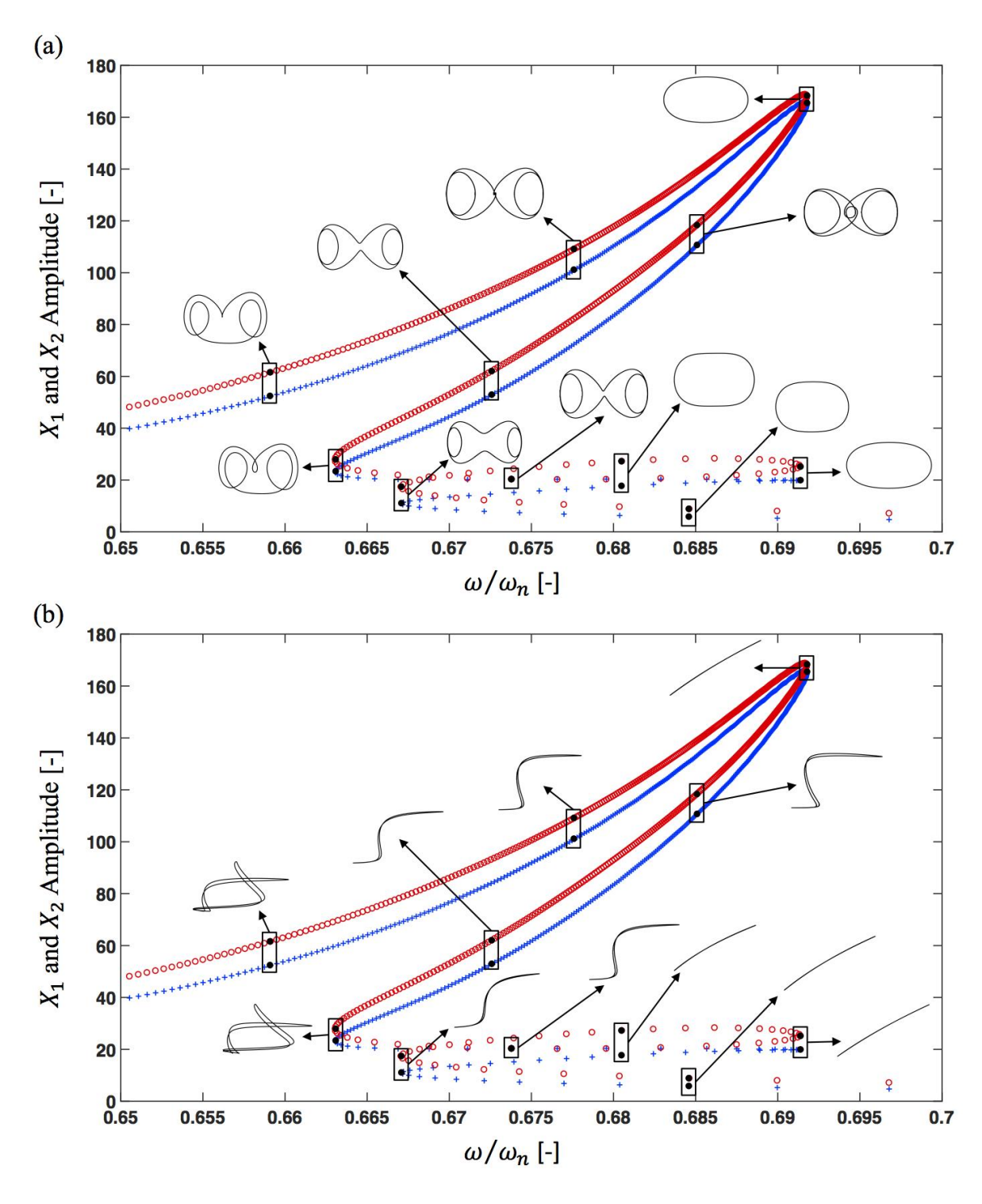


Figure 9: Nonlinear frequency response curves in the vicinity of first natural frequency for  $\alpha=0.01$ . (a) Phase portraits of relative motion; (b) Phase portraits of kinetic energies. Key: +,  $X_1$  amplitude,  $\bigcirc$ ,  $X_2$  amplitude.

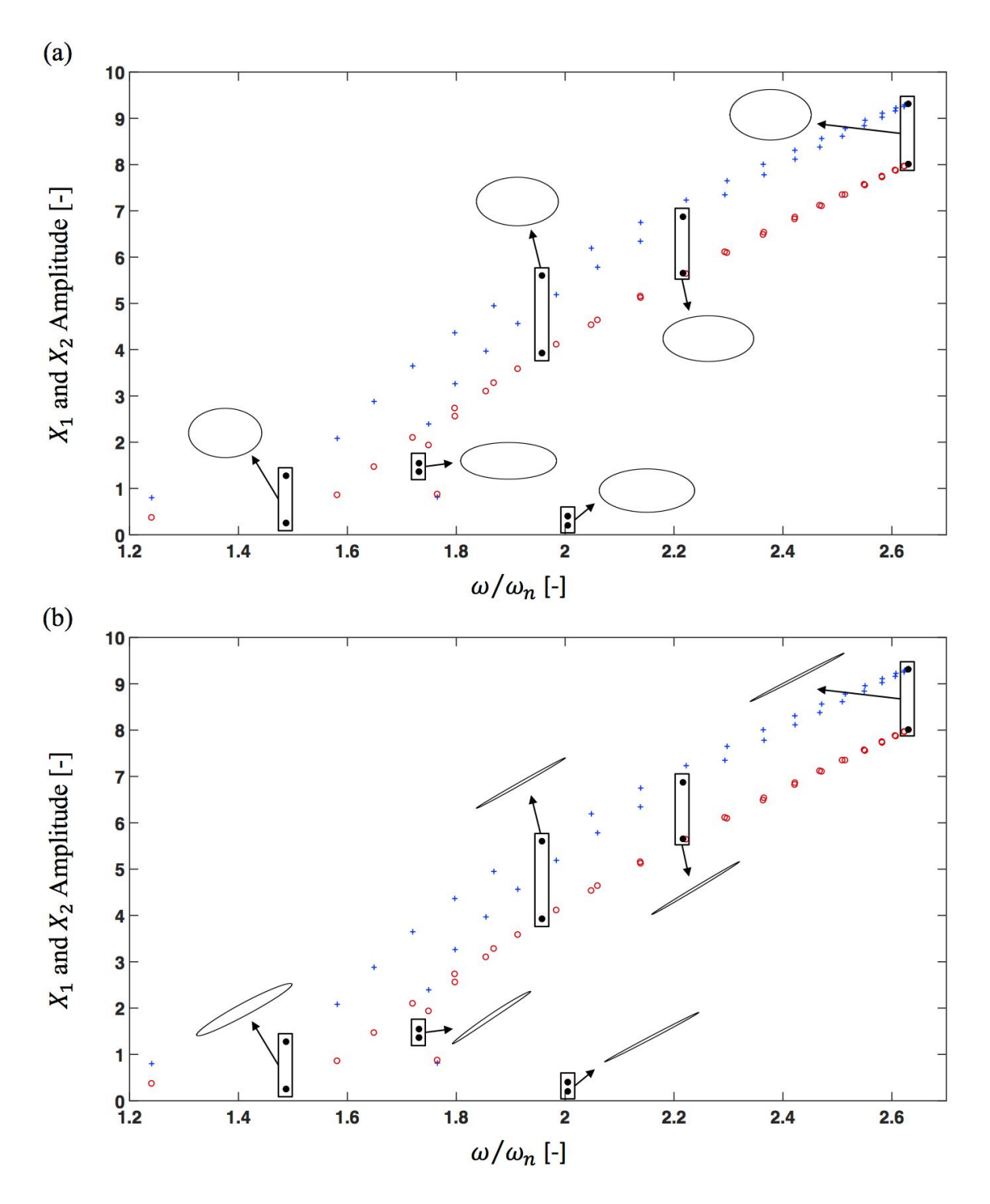


Figure 10: Nonlinear frequency response curves in the vicinity of second natural frequency for  $\alpha = 0.01$ . (a) Phase portraits of relative motion; (b) Phase portraits of kinetic energies. Key: +,  $X_1$  amplitude, O,  $X_2$  amplitude.

## 5 CONCLUSION

In this study, dynamic behavior of two sub-systems that are connected through a nonlinear elastic path is investigated. First, the nonlinear governing equations are converted into non-dimensional form, and the nonlinear frequency response curves at different levels of nonlinearity are constructed using the multi-term harmonic balance method. It is observed that

additional branches in the frequency response curves emerge at strong nonlinearities, though these occur only around the first natural frequency. The behavior around the second natural frequency is a simple bending of the backbone response curve toward higher frequencies due to the hardening type stiffness. Finally, the nonlinear governing equations (in the non-dimensional form) are numerically solved at selected excitation frequencies and nonlinearity levels. The period doubling (or halving) behavior is observed with a change in the excitation frequency. Furthermore, the kinetic energy exchange mechanism between two sub-systems also changes with respect to the excitation frequency and/or level of nonlinearity. In conclusion, an improved insight into the energy exchange within a nonlinear system is obtained depending on the excitation frequency and/or the extent of nonlinearity.

#### **ACKNOWLEDGEMENTS**

We acknowledge the Smart Vehicle Concepts Center (https://svc.osu.edu) and the National Science Foundation Industry/University Cooperative Research Centers program in USA (www.nsf.gov/eng/iip/iucrc) for supporting this fundamental study. The second author also thanks the OSU Emeritus Academy for partially supporting the research.

#### REFERENCES

- [1] Y. Starosvetsky and O.V. Gendelman. Dynamics of a strongly nonlinear vibration absorber coupled to a harmonically excited two-degree of freedom system. *Journal of Sound and Vibration*, 312, 234-256, 2008.
- [2] M. Kurt, M. Eriten, D.M. McFarland, L.A. Bergman and A.F. Vakakis. Frequency-energy plots of steady-state solutions for forced and damped systems, and vibration isolation by nonlinear mode localization. *Communications in Nonlinear Science and Numerical Simulation*, 19, 2905-2917, 2014.
- [3] X. Jiang, D.M. McFarland, L.A. Bergman and A.F. Vakakis. Steady-state passive nonlinear energy pumping in coupled oscillators: Theoretical and experimental results. *Nonlinear Dynamics*, 33, 87-102, 2003.
- [4] D. Andersen, Y. Starosvetsky, A.F. Vakakis and L. Bergman. Dynamic instabilities in coupled oscillators induced by geometrically nonlinear damping. *Nonlinear Dynamics*, 67, 807-827, 2012.